

Ultrahigh-Intensity Laser-Produced Plasmas as a Compact Heavy Ion Injection Source

K. Krushelnick, E. L. Clark, R. Allott, F. N. Beg, C. N. Danson, A. Machacek, V. Malka, Z. Najmudin, D. Neely, P. A. Norreys, M. R. Salvati, M. I. K. Santala, M. Tatarakis, I. Watts, M. Zepf, and A. E. Dangor

Abstract—The possibility of using high-intensity laser-produced plasmas as a source of energetic ions for heavy ion accelerators is addressed. Experiments have shown that neon ions greater than 6 MeV can be produced from gas jet plasmas, and well-collimated proton beams greater than 20 MeV have been produced from high-intensity laser solid interactions. The proton beams from the back of thin targets appear to be more collimated and reproducible than are high-energy ions generated in the ablated plasma at the front of the target and may be more suitable for ion injection applications. Lead ions have been produced at energies up to 430 MeV.

Index Terms—Heavy ion accelerators, ion accelerators, ion source, laser-plasma interactions.

I. INTRODUCTION

OVER the past several years, there have been significant advances in the use of high-power, short pulse lasers [1]. In particular, the potential of such lasers for applications in particle acceleration [2], X-ray generation [3], and inertial confinement fusion [4] seems promising. The complex interactions between matter and high-intensity laser light can produce electrons at energies greater than 100 MeV and gamma rays up to tens of MeV. However, it may also be possible to use such laser systems to produce plasmas that can be used as a source of energetic heavy ions for injection into ion storage rings and colliders.

In this paper, we will discuss some recent experiments that address the feasibility and advantages of this approach for producing a source of energetic ions. There has been considerable previous work on the use of laser-produced plasmas as such a source of highly ionized heavy ions [5]–[7], [18], where it was found that laser ion sources have several advantages over other methods, such as electron–cyclotron sources, electron beam ion sources, and metal vapor vacuum arcs. Heavy ions (of a few MeV) have been generated by the ablated plasma created by low-intensity solid target interactions, after which they were accelerated by an RF quadrupole to energies of a few hundred MeV before injection into an ion storage ring. Our research in-

dicates that through the use of “table top” chirped pulse amplification (CPA) laser systems, it may be possible to produce heavy highly ionized ions at energies approaching a GeV in sufficient quantities to directly inject into ion storage rings. Such heavy ions can be generated in a gas jet plasma (which allows high repetition rates) or through solid target interactions (which may provide a more collimated and energetic source of such heavy ions). We present angular emission data and ion energy spectra as well as a possible source geometry.

II. INTERACTIONS WITH UNDERDENSE PLASMAS

Accelerated ions can be produced in underdense “gas jet” interactions via the “Coulomb explosion” of a high-intensity laser-produced plasma [8]. In this situation, ions are accelerated by electrostatic forces caused by charge separation induced by the laser ponderomotive pressure. In these experiments, we have measured peak ion energies of 1.0 MeV for deuterium gas interactions, 3.6 MeV for helium interactions, and greater than 6 MeV for interactions with neon.

As a high-intensity laser pulse propagates through an underdense plasma, the strong ponderomotive force of the laser forces electrons from the region of highest intensity. Ions are less affected by this ponderomotive force because of their larger mass; however, during the laser pulse, these ions will be given a impulse perpendicular to the axis of laser propagation that is produced by the large space-charge forces caused by charge separation. After the pulse passes, the plasma electrons will return to their original positions on a timescale of about $1/\omega_{pe}$, (where $\omega_{pe} = 4\pi n_e e^2/m_e$ is the electron plasma frequency); however, the lateral momentum given to the ions will be retained and they will continue moving out of the plasma, carrying low-energy electrons with them. The energy of these ions is thus directly related to the intensity of the focused laser pulse. The maximum energy that can be gained by an ion during these interactions is simply given as the relativistic ponderomotive energy, $U = Zm_e c^2(\gamma - 1)$, where Z is the ion charge and γ is the relativistic factor of the electron quiver motion in the laser field.

Our experiments were performed using the CPA arm of the VULCAN laser system at the Rutherford Appleton Laboratory. This system produces laser pulses having an energy of up to 50 J and a duration of 0.9–1.2 ps at a wavelength of 1.054 μm (Nd: Glass). The laser pulse was focused into a gas jet target (4-mm nozzle diameter) using an $f/4$ off-axis parabolic mirror. When helium was used as the target gas, the plasma had an electron density up to about $5 \times 10^{19} \text{ cm}^{-3}$. Deuterium and neon were also used as target gases.

Manuscript received October 2, 1999; revised February 24, 2000.

K. Krushelnick, F. N. Beg, Z. Najmudin, M. R. Salvati, M. I. K. Santala, M. Tatarakis, I. Watts, M. Zepf, and A. E. Dangor are with the Imperial College, SW7 2BZ, London, U.K.

E. L. Clark is with the Radiation Physics Department, AWE plc, RG7 4PR, Aldermaston, U.K., and the Imperial College, SW7 2BZ, London, U.K.

R. Allott, C. N. Danson, D. Neely, and P. A. Norreys are with the Rutherford Appleton Laboratory, Chilton, Didcot, OX11 0QX Oxon, U.K.

A. Machacek is with the Department of Physics, University of Oxford, OX1 3PU Oxford, U.K.

V. Malka is with LULI, CNRS-CEA, École Polytechnique-Université Pierre et Marie Curie, 91128 Palaiseau Cedex, France.

Publisher Item Identifier S 0093-3813(00)07243-X.

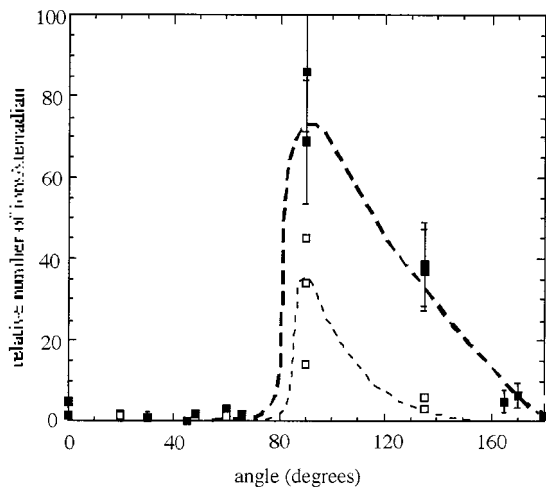


Fig. 1. Angular emission of energetic ions, where 0° is along the direction of laser propagation. Dark line: distribution of helium ions with energy greater than 400 keV; Light line: distribution of helium energy greater than 2 MeV (shown $\times 10$). Note that lines are drawn as visual aid only.)

The angular distribution of ions emitted during such high-intensity laser plasma interactions was recorded using CR-39 track detectors placed at various places surrounding the interaction region and that are sensitive to energetic ions greater than about 100 keV/nucleon [9]. As an energetic ion collides with the detector, it causes structural damage in the material so that an observable track can be recorded for each ion. In this way, the total number of ions can be counted.

It was found in these experiments that there was no significant variation in ion emission in the azimuthal direction (i.e., changing the laser polarization had little effect). However, a distinct peak was observed in the emission of ions with energies greater than 300 keV at 90° to the axis of propagation. Measurements of the ion emission at higher energies were also obtained by using CR-39 track detectors covered with thin aluminum filters ($2 \mu\text{m}$). Such filters block all signal from helium ions below about 2 MeV in energy.

Averaged measurements over four shots are shown in Fig. 1. Clearly, the majority of ion emission occurs in the 90° direction, although the emission lobe also extends in the backward direction somewhat. Emission at energies greater than 2 MeV shows a narrower lobe in the 90° direction. The spectrum of the energetic ions was also measured using a Thomson parabola ion spectrometer that spatially separates ion species having different charge to mass ratios through the use of parallel electric and magnetic fields. CR-39 was used as the detector. Typical experimentally measured spectra are shown in Fig. 2 for helium interactions and Fig. 3 for neon interactions.

For the helium interactions, it was found that approximately 0.25% of the incident laser energy is transferred to ions having greater than 300 keV of energy. It is interesting to note that in helium plasmas, both He^{1+} and He^{2+} ions were observed with very high energy. In the interaction region, helium ions are completely ionized because the intensity required to directly field ionize He^{1+} is about 10^{16} W/cm^2 . This implies that the He^{1+} is generated by charge-exchange/recombination of ions as they travel out of the gas jet to the detector. In neon interactions, the

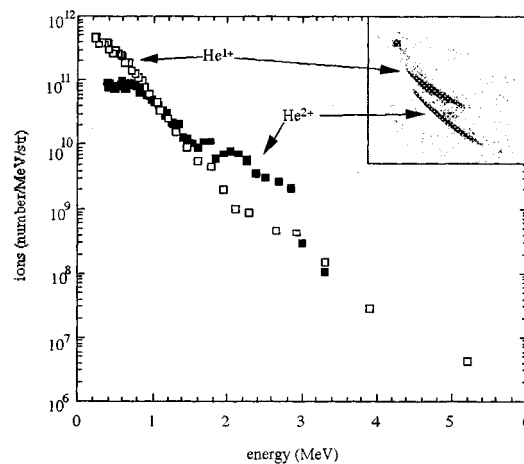


Fig. 2. Typical ion spectrum from helium interaction (90°) (Thomson parabola data are shown inset).

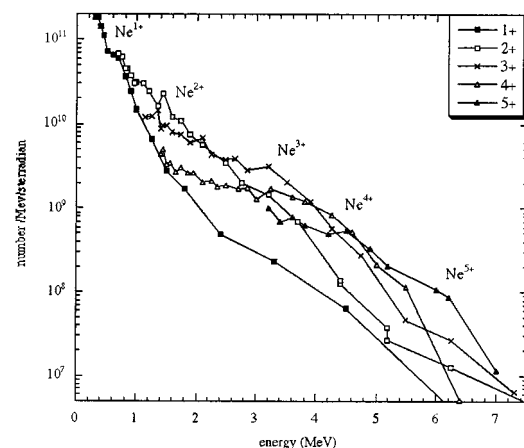


Fig. 3. Typical ion spectrum from neon interaction (90°).

atoms can be stripped up to the Ne^{8+} stage from direct field ionization; however, only neon species up to Ne^{5+} were observed in our experiment (see Fig. 3), also indicating significant charge exchange/recombination.

The maximum ion energy, such that there were more than 10^8 ions/MeV/steradian, was found to be 3.6 MeV for helium, 1.0 MeV for deuterium, and greater than 6 MeV for neon. It should be noted that ionization-induced defocusing of the laser pulse in the neon plasma appeared to reduce the peak energy of neon ions obtainable from these interactions.

III. SOLID TARGET INTERACTIONS

Major advances in understanding the mechanisms of energetic ion emission were made during early inertial confinement fusion experiments using high-power CO_2 lasers [10] and results from those experiments (at irradiances of about $10^{18} \text{ Wcm}^{-2} \mu\text{m}^2$) [11] indicated that ions with energies greater than 2 MeV/nucleon could be produced from interactions with solid density plasmas. The principal diagnostics employed in those measurements were Faraday cups and charge collection cups. Using such time of flight methods only, information concerning the ion velocity (energy/nucleon) can be obtained.

We have also performed experiments to examine the generation of high-energy ions from interactions with solid density plasmas at the Rutherford Appleton Laboratory. In these experiments, the VULCAN beam was focused using an $f/4$ off-axis parabolic mirror onto a thin ($125\text{-}\mu\text{m}$) aluminum target positioned at 45° to the axis of laser propagation. The intensity on target was up to $5 \times 10^{19} \text{ W/cm}^2$. Both behind the target (25-mm distance) and at the front of the target (70 mm), we placed “sandwich detectors” aligned with the normal to the target. These detectors consist of several pieces of radiochromic film (RCF) and CR39 plastic track detectors placed back to back. The principal ions detected were energetic protons or carbon ions that were either from hydrocarbon contamination of the front or rear target surfaces (which has been observed in previous experiments [12]).

RCF is a transparent material (typically nylon) that is coated with an organic dye. Upon exposure to ionizing radiation, the film undergoes a color change. The optical density of the film is subsequently measured at a particular wavelength and is calibrated against dose (Gy) using a known ^{60}Co source. The equivalent dose from protons at a particular energy is calculated, and hence, the total number of protons passing through the film at each point can be determined.

In this experiment, the CR39 detectors only recorded signals caused by protons because the first piece of RCF ($110\text{-}\mu\text{m}$ thick) in the “sandwich” will transmit protons having energies greater than 2.8 MeV, but will stop all but the highest energy aluminum and carbon ions. The stopping range of protons in CR39 and radiochromic film is easily calculated, and consequently, this allows a direct determination of the energy range for those protons that produce a particular series of pits. CR39/RCF “sandwich” detectors can therefore provide both spatial and spectral information of protons emitted during the interaction.

Fig. 4(a) shows a scanned image from the front piece of RCF in the “sandwich” detector from a typical shot at $I \sim 5 \times 10^{19} \text{ W/cm}^2$ from the rear of a target. The film contains signal only within a well-defined radius from the central hot-spot. The angle subtended by the perimeter of this circle covers a cone half angle of 30° , and the mark at the center of the film indicates a region where the film has been saturated. Fig. 4(b)–(e) shows the emission pattern observed on the CR39 from this shot for various energy ranges of ions (i.e., different pieces in the “sandwich”). RCF is also sensitive to both electrons and X-rays, which are generated during the interaction [13], [19]; however, it is clear from the images shown in Fig. 4(b)–(e) that the signal on the RCF coincides with that on the CR39, which is sensitive only to ions. Therefore, it is likely that the signal on the front piece of film is predominantly caused by energetic ion emission. Using this assumption, the total number of protons emitted with energies greater than 2 MeV can be estimated and was found to be approximately 10^{12} per shot.

The ion signal on the CR39 exhibits a ring pattern with decreasing diameter for increasing ion energy up to a maximum energy of 17.6 MeV. The central position of each ring is coincident with the direction of the target normal. The “ion ring” structure on the CR39 was observed consistently from shots at an intensity of $\sim 5 \times 10^{19} \text{ W/cm}^2$. The central hot spot on the RCF is correlated with the position of the highest energy ions on

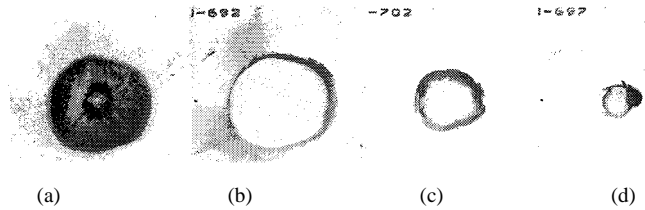


Fig. 4. Ring structure observed on back RCF/CR39 “sandwich” track detectors: (a) radiochromic film (front surface), (b) tracks on CR39 from 3-MeV, (c) 8.9-MeV, (d) 11.6-MeV, and (e) 17.6-MeV protons (track detectors were $5 \text{ cm} \times 5 \text{ cm} \times 0.75 \text{ mm}$ thick).

the CR39, which exhibit collimated propagation, and the outer extreme of the RCF displays an abrupt decrease in signal level, which corresponds to a sharp low energy cutoff, below which no protons are observed.

It is possible that this relationship between the energy of the emitted protons and the angle at which they are emitted is caused by large azimuthal magnetic fields within the solid target material that develop and persist during the first few picoseconds after the laser pulse. The protons are consequently deflected like charged particles in a magnetic spectrometer. It is clear that such magnetic fields must be generated by an electron current, which would tend to focus a beam of electrons, but defocus or scatter ions. Such large fields have been predicted [14], and have been shown to contribute to the focusing of electrons at the rear of such targets resulting in plasma formation [15].

Simultaneously, measurements of the gamma-ray spectrum using a gamma-ray spectrometer (scintillators/photo-multipliers) as well as through the use of nuclear activation techniques [20], [21], implied that the hot electron temperature was in the range of 1 to 2 MeV. The spectrum of high-energy electrons propagating through the $125\text{-}\mu\text{m}$ targets was also measured, and it was found to extend to energies greater than 20 MeV. It is likely that part of the return current required for propagation of the hot electrons through the target material is provided by protons from the front surface plasma that are pulled along with these electrons as they propagate into the plasma. From these measurements, we have been able to infer the structure and magnitude of the magnetic field generated within a solid target during an ultrahigh-intensity laser interaction [16].

These results are in contrast to measurements of the heavy ion and proton spectra in the forward direction (i.e., in the plume of ablated plasma), which were similarly recorded with high spatial and spectral resolution. In this direction, we have observed the formation of a lower energy ring structure composed of protons ($\sim 4 \text{ MeV}$) and heavy ions that is probably created by magnetic fields that exist in the expanding plasma and a higher energy population that exhibits a less well-defined structure.

To measure both the heavy ion and proton spectra, a Thomson parabola ion spectrometer using CR39 plastic nuclear track detectors was situated at an angle of 20° from the target normal. In addition, the spectral and spatial distribution of the protons emitted from the interaction was determined by placing a “sandwich” of several pieces of radiochromic film and CR39 detectors in front of the target—similar to that which was used at the back.

The CR39/radiochromic film pack was covered with a 20- μm thick piece of aluminum and was aligned with the target at a distance of 70 mm from the surface, the center of which coincided with the target normal. The target was again a 125- μm thick piece of aluminum. Almost no heavy ions penetrate the first layer of radiochromic film and the signal on the subsequent pieces of CR39 is largely from energetic protons originating from hydrocarbon contaminants on the front surface of the target.

In this “sandwich” target, the first piece of radiochromic film shows a ring structure that is consistent with a ring of low energy (≤ 4 -MeV) protons recorded on the following piece of CR39. The center of the ring does not coincide with the target normal, but is shifted by about 10° back toward the direction of the incident laser, and down slightly. Overall, the low-energy ion emission occurs within a 20° cone (the plasma plume) and is characterized by a fine-scale filamentary structure. The surface of the CR39 records some of the proton signal from the ring, but little additional signal is seen.

Higher energy protons were measured by the subsequent pieces of CR39 in the “sandwich,” which are separated by a single piece of radiochromic film. The energies at these surfaces are 11 MeV and 13 MeV, respectively. Here, no ring structure is observed and the protons cover an emission area that gets smaller as the energy of the protons increases, but has no apparent correlation with the lower energy component. Measurements of protons of energies up to 18 MeV and 20 MeV were made using a similar technique; however, they were observed to be much less collimated than were those measured at the back of the target. Similar data (which also showed the same low-energy ring structure) was consistently measured over a series of shots. Simultaneous measurements at the front and the rear of the target indicate that the maximum proton energies are almost the same in both directions (see below).

It is likely that the lower energy component of the proton emission is produced during the expansion phase of the plasma. During this period, temperature gradients along the target surface combined with nonparallel density gradients from the expanding plasma produce self-generated magnetic fields [17]. These fields may affect the plasma [15] as it expands, thus, forming the “ion ring,” as discussed earlier. These ions, which include protons of up to 4 MeV, have energies that are consistent with plasma expansion velocities as measured by optical probing [15]. The magnetic pressure along the target normal collimates the expanding plasma at the laser spot to produce a plasma jet containing low-energy ions and electrons that can be seen as a bright central feature. This plasma jet is likely formed before the toroidal plasma formation and in the direction away from the target along the normal to the surface. The ring of plasma is formed as the magnetic field is generated in the ablating plume and is recorded as low-energy protons and ions on the radiochromic film. Such plasma formation has been observed in MHD simulations and in previous experiments [15]. A fine-scale filamentary structure can be seen on the radiochromic film at the edge of the ring, which is unlike the images recorded on radiochromic film at the rear of the target.

The higher energy component of the ion emission appears to be qualitatively different from the lower energy component and

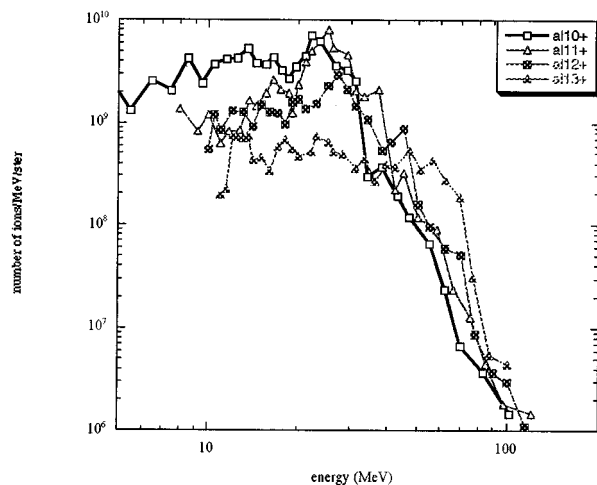


Fig. 5. Typical aluminum ion spectrum from front surface plasma during interactions at $\sim 3 \times 10^{19}$ W/cm 2 .

does not exhibit a ring structure. It is possible that these ions are produced near the critical surface where large electrostatic fields can be generated via plasma wave generation (via a mechanism such as resonance absorption). The interaction process is therefore capable of producing equivalent maximum proton energies in both directions at the front target surface. The number of protons above 1 MeV is about the same as that measured at the rear of the target. The fact that the very highest energy ions in the plasma plume have a similar energy to those recorded at the back of the target suggests that they are not produced in the ablated plume, but they are generated by large electrostatic fields near the critical density surface, which may accelerate ions in both directions.

The detailed energy spectra of ions emitted during these interactions were obtained using the Thomson parabola ion spectrometer. Previous measurements suggest that the dominant component of the ion emission is protons, however, it is clear that a substantial contribution is from other ion species. Measurements of ion emission from lead targets indicate Pd-like Pb^{36+} ions up to 220 MeV and Xe-like Pb^{46+} ions up to 430 MeV. Fully stripped aluminum (Fig. 5) and carbon ions up to 150 MeV and 90 MeV were also measured. The total number of Al ions greater than 10 MeV was estimated to be $\sim 10^{11}$ ions/sterradian.

These experiments suggest that there are two components to proton and ion production. The lower energy part is formed many picoseconds after the laser pulse as the heated plasma ablates and is strongly influenced by the magnetic field generation to be in the plasma. In contrast, the higher energy component is likely generated during the laser interaction period.

IV. ION SOURCES

The requirements for an ion source are that it be able to operate at repetition rates of at least 1 Hz, that it have short pulse length, high luminosity, and that it be flexible to make available a wide variety of ionized species. It is likely that an ion source using high-intensity laser-produced plasmas could meet these requirements easily. The pulse length of ions must be less than the revolution time for ions in a synchrotron.

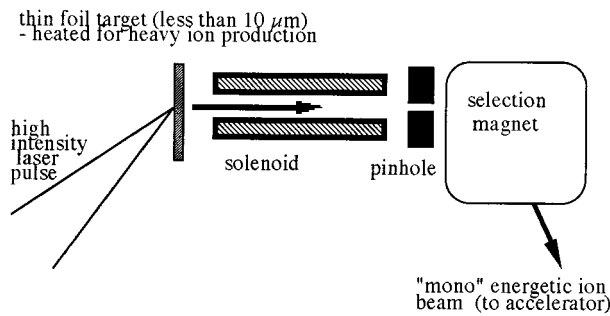


Fig. 6. Schematic of possible high intensity laser-plasma ion injector geometry.

From the above discussion, it is clear that there are distinct advantages to the use of high-intensity lasers for ion acceleration. If gas jets are used as the target, it seems likely that high repetition sources of highly ionized noble gases having energies of up to 10 MeV can be produced. The disadvantage of this approach is that the ion energies are typically low and that the ions are emitted with a broad angular distribution so that a complicated collection scheme may be necessary. There are also fewer energetic ions emitted from underdense interactions for similar focused laser intensities.

For solid target interactions, it appears that nonlinear acceleration mechanisms in the interaction region can produce high-energy ions. However, it is not clear how the peak ion energy scales with incident laser intensity. In the past, laser-produced ion sources have used ions produced in the ablated plasma plume, and while this seems to be possible using very intense laser pulses, a better design for a high-intensity ion source would involve the use of the forward-propagating beam of ions. Such ions are almost as energetic as the ions emitted in the plume, and it also appears that magnetic fields generated inside thin targets tend to focus and collimate the highest energy ions after they are emitted. A possible design for a high-intensity laser/dense plasma ion source is shown in Fig. 6. The energies of the emitted ions and the observed angular emission of these sources suggest that perhaps the linac pre-acceleration stage can be avoided with the use of high-intensity laser ion sources, although clearly further work is required to determine the reproducibility of the angular emission pattern and of the energy spectrum of emitted ions.

The authors would like to acknowledge the technical assistance of the VULCAN operations team in these experiments.

REFERENCES

- [1] M. Perry and G. Mourou, "Terawatt to petawatt subpicosecond lasers," *Science*, vol. 264, pp. 917–924, 1994.
- [2] E. Esarey, P. Sprangle, J. Krall, and A. Ting, "Overview of plasma-based accelerator concepts," *IEEE Trans. Plasma Sci.*, vol. 24, p. 252, 1996.
- [3] N. H. Burnett and G. D. Enright, "Population inversion in the recombination of optically-ionized plasmas," *IEEE J. Quant. Electron.*, vol. 26, pp. 1797–1808, 1990.
- [4] M. Tabak, J. Hammer, M. E. Glinsky, W. L. Kruer, S. C. Wilks, J. Woodworth, E. M. Campbell, M. D. Perry, and R. J. Mason, "Ignition and high gain with ultrapowerful lasers," *Phys. Plasmas*, vol. 1, pp. 1626–1634, 1994.
- [5] M. Lezius, S. Dobosz, D. Normand, and M. Schmidt, "Explosion dynamics of rare gas clusters in strong laser fields," *Phys. Rev. Lett.*, vol. 80, pp. 261–264, 1998.
- [6] J. Collier, G. Hall, H. Haseroth, H. Kugler, A. Kuttenger, K. Langbein, R. Scrivens, T. Sherwood, J. Tambini, B. Sharkov, A. Shumshurov, and K. Masek, "The CERN laser-ion source," *Lasers Particle Beams*, vol. 14, pp. 283–292, 1996.
- [7] P. Fournier, G. Gregoire, H. Kugler, H. Haseroth, N. Lisi, C. Meyer, P. Ostroumov, J. C. Schnuriger, R. Scrivens, F. V. Rodriguez, B. H. Wolf, S. Homenko, K. Makarov, Y. Satov, A. Stepanov, S. Kondrashev, B. Sharkov, and A. Shumshurov, "Status of the CO₂ laser ion source at CERN," *Rev. Sci. Instrum.*, vol. 71, pp. 924–926, 2000.
- [8] K. Krushelnick, E. Clark, Z. Najmudin, M. Salvati, M. I. K. Santala, M. Tatarakis, A. E. Dangor, V. Malka, D. Neely, R. Allott, and C. Danson, "Multi-MeV ion production from high intensity laser interactions with underdense plasmas," *Phys. Rev. Lett.*, vol. 83, pp. 737–740, 1999.
- [9] A. P. Fews, "Flexible analysis of etched nuclear-particle tracks," *Nucl. Instrum. Methods Phys. Res., Sect.*, vol. 72, pp. 91–103, 1992.
- [10] R. L. Carlson, J. P. Carpenter, D. E. Casperson, R. B. Gibbon, R. P. Godwin, R. F. Haglund, J. A. Hanlon, E. L. Jolly, and T. F. Stratton, "HELIOS—A 15 TW carbon dioxide laser fusion facility," *IEEE J. Quantum Electron.*, vol. QE-17, pp. 1662–1678, 1981.
- [11] S. J. Gitomer, R. D. Jones, F. Begay, A. W. Ehler, J. F. Kephart, and R. Kristal, "Fast ions and hot electrons in the laser plasma interaction," *Phys. Fluids*, vol. 29, pp. 2679–2688, 1986.
- [12] A. P. Fews, P. A. Norreys, F. N. Beg, A. R. Bell, A. E. Dangor, C. N. Danson, P. Lee, and S. J. Rose, "Plasma ion emission from high intensity intensity picosecond laser pulse interactions with solid targets," *Phys. Rev. Lett.*, vol. 73, pp. 1801–1804, 1994.
- [13] P. A. Norreys, M. I. K. Santala, E. Clark, M. Zepf, I. Watts, F. N. Beg, K. Krushelnick, M. Tatarakis, A. E. Dangor, X. Fang, P. Graham, T. McCanny, R. P. Singhal, K. W. D. Ledingham, A. Creswell, D. C. W. Sanderson, J. Magill, A. Machacek, J. S. Wark, R. Allott, B. Kennedy, and D. Neely, "Observation of a highly directional gamma-ray beam from ultra-short, ultra-intense laser pulse interactions with solids," *Phys. Plasmas*, vol. 6, p. 2150, 1999.
- [14] J. R. Davies, A. R. Bell, M. G. Haines, and S. M. Guerin, "Short-pulse high-intensity laser-generated fast electron transport into thick solid targets," *Phys. Rev. E*, vol. 56, pp. 7193–7203, 1997.
- [15] M. Tatarakis, J. R. Davies, P. Lee, P. A. Norreys, N. G. Kassapakis, F. N. Beg, A. R. Bell, M. G. Haines, and A. E. Dangor, "Plasma formation on the front and rear of plastic targets due to high-intensity laser-generated fast electrons," *Phys. Rev. Lett.*, vol. 81, no. 5, pp. 999–1002, 1998.
- [16] E. L. Clark, K. Krushelnick, J. R. Davies, F. N. Beg, M. I. K. Santala, M. Tatarakis, I. Watts, M. Zepf, A. E. Dangor, P. A. Norreys, and A. Machacek, "Measurements of energetic proton transport through magnetized plasma from intense laser interactions with solids," *Phys. Rev. Lett.*, vol. 84, pp. 670–673, 2000.
- [17] J. A. Stamper, "Review on spontaneous magnetic fields in laser-produced plasma-phenomena and measurements," *Laser Particle Beams*, vol. 9, pp. 841–862, 1991.
- [18] T. Ditmire, J. W. G. Tisch, E. Springate, M. B. Mason, N. Hay, J. P. Marangos, and M. H. R. Hutchinson, "High energy ion explosion of atomic clusters: Transition from molecular to plasma behavior," *Phys. Rev. Lett.*, vol. 78, pp. 2732–2735, 1997.
- [19] F. N. Beg, A. R. Bell, A. E. Dangor, C. N. Danson, A. P. Fews, M. E. Glinsky, B. A. Hammel, P. Lee, P. A. Norreys, and M. Tatarakis, "A study of picosecond laser-solid interactions up to 10^{19} W cm⁻²," *Phys. Plasmas*, vol. 4, pp. 447–457, 1997.
- [20] M. I. K. Santala, E. Clark, I. Watts, F. N. Beg, M. Tatarakis, M. Zepf, K. Krushelnick, A. E. Dangor, T. McCanny, I. Spencer, R. P. Singhal, K. W. D. Ledingham, S. C. Wilks, A. C. Machacek, J. S. Wark, R. Allott, R. J. Clarke, and P. A. Norreys, "The effect of the plasma density scale length on the direction of fast electrons in relativistic laser-solid interactions," *Phys. Rev. Lett.*, vol. 84, pp. 1459–1462, 2000.
- [21] K. W. D. Ledingham, I. Spencer, T. McCanny, R. P. Singhal, M. I. K. Santala, E. Clark, I. Watts, F. N. Beg, M. Zepf, K. Krushelnick, M. Tatarakis, A. E. Dangor, P. A. Norreys, R. Allott, D. Neely, R. J. Clarke, A. Machacek, J. S. Wark, A. J. Cresswell, D. C. W. Sanderson, and J. Magill, "Photo-nuclear physics when a multiterawatt laser pulse interacts with solid targets," *Phys. Rev. Lett.*, vol. 84, pp. 899–902, 2000.

K. Krushelnick, photograph and biography not available at the time of publication.

E. L. Clark, photograph and biography not available at the time of publication.

R. Allott, photograph and biography not available at the time of publication.

P. A. Norreys, photograph and biography not available at the time of publication.

F. N. Beg, photograph and biography not available at the time of publication.

M. R. Salvati, photograph and biography not available at the time of publication.

C. N. Danson, photograph and biography not available at the time of publication.

M. I. K. Santala, photograph and biography not available at the time of publication.

A. Machacek, photograph and biography not available at the time of publication.

M. Tatarakis, photograph and biography not available at the time of publication.

V. Malka, photograph and biography not available at the time of publication.

I. Watts, photograph and biography not available at the time of publication.

Z. Najmudin, photograph and biography not available at the time of publication.

M. Zepf, photograph and biography not available at the time of publication.

D. Neely, photograph and biography not available at the time of publication.

A. E. Dangor, photograph and biography not available at the time of publication.